About the elongation at break of unfilled natural rubber elastomers

F. Grasland, L. Chazeau, J.-M. Chenal, J. Caillard, R. Schach

▶ **To cite this version:**

F. Grasland, L. Chazeau, J.-M. Chenal, J. Caillard, R. Schach. About the elongation at break of unfilled natural rubber elastomers. Polymer, 2019, 169, pp.195-206. 10.1016/j.polymer.2019.02.032 . hal-02405451

HAL Id: hal-02405451
https://hal.science/hal-02405451

Submitted on 22 Oct 2021

HAL is a multi-disciplinary open access archive for the deposit and dissemination of scientific research documents, whether they are published or not. The documents may come from teaching and research institutions in France or abroad, or from public or private research centers.

L'archive ouverte pluridisciplinaire **HAL**, est destinée au dépôt et à la diffusion de documents scientifiques de niveau recherche, publiés ou non, émanant des établissements d'enseignement et de recherche français ou étrangers, des laboratoires publics ou privés.

Distributed under a Creative Commons Attribution - NonCommercial 4.0 International License

Version of Record: https://www.sciencedirect.com/science/article/pii/S0032386119301636
Manuscript_61c62d26eb21791df90debabf1f67dbd

ABOUT THE ELONGATION AT BREAK OF UNFILLED NATURAL RUBBER ELASTOMERS

François Grasland[a], Laurent Chazeau[a*], Jean-Marc Chenal[a], Julien Caillard[b] and Regis Schach[b]

[a] Univ Lyon, INSA Lyon, CNRS, MATEIS UMR5510, F-69621, Lyon, France

[b]Centre de technologies, Manufacture Française des Pneumatiques Michelin, 63040 Clermont Ferrand Cedex 9, France

[*]Correspondance email : laurent.chazeau@insa-lyon.fr

ABSTRACT

This paper presents the characterization of the mechanical properties, of the ability to crystallize thermally or under strain, and of the Elastically Active Chains (EAC) network of Natural Rubber elastomer, whose EAC average density and length distribution were modified by thermo-oxidative ageing. EAC length distribution is not a critical parameter for λ_{break} in elastomers which do not crystallize (as far as the quantity of free and dangling chains stays negligible, which is the case in this study). However, it becomes important in crystallizable materials, since it controls the chains quantity which can be stretched enough to crystallize. When this quantity is large enough, the material can be stretched up to λ_c, and the crystallization process will enable to increase both λ_{break} and σ_{break}. Conversely when it is too low, λ_{break} is seemingly mainly governed by the average EAC density and a power law then links both quantities.

Keywords: Elastomer, rupture properties, microstructure, strain-induced crystallization, network heterogeneities

© 2019 published by Elsevier. This manuscript is made available under the CC BY NC user license
https://creativecommons.org/licenses/by-nc/4.0/

1. INTRODUCTION

Understanding rupture properties evolution of elastomers during their use is obviously an important challenge as these materials are largely used in many applications. For this reason, literature on this topic is very abundant, which tries to relate the ultimate properties to the elastomer network structure. There is a general consensus on the fact that the length of the elastically active chain (EAC) is an important parameter for the elongation at break. In the case of monomodal distribution of elastomer chains in a perfect, (i.e. without defects) networks, all the chains reaching their maximum extensibility at the same time, the elongation at break should be proportional to the ratio of their contour length over their end to end distance at equilibrium. With the assumption of initial Gaussian chains, this should lead to a proportionality of λ_{break} to the square root of the number of Kuhn segment in the EAC chain. With a monomodal distribution, this immediately gives a proportionality to $\nu^{-1/2}$ where ν is the EAC density. Nevertheless, EAC chains length may be distributed and this distribution could be spatially not stochastic. For instance, some percolating paths of shorter chains could therefore be created during the elastomer curing and may control the macroscopic rupture of the material. Real elastomers can also contain elastically non-active chains, and sol fraction which also perturbs the affine extension of the EAC, and may favor energy dissipation (therefore increasing the energy needed for the rupture mechanisms). Thus, the simple equation proposed by Kuhn [1] is rarely verified in real elastomers [2], [3], or when this is the case, only on a limited domain. Actually, a good fit of $\lambda_{break}(\nu)$ data usually needs the addition of a constant term, whose value and interpretation is not clear [4], [5].

It is however remarkable that several literature data about $\lambda_{break}(\nu)$ can be fitted by a power law [2], [6], [7], [42] although, to the authors knowledge, no explanation is given for the found exponents. These power law may actually be related to another important parameter for the material rupture, which is the presence of defects such as preexisting small cracks or cavities. The vision of a material breaking instantaneously in two pieces as suggested by the previous paragraph (with the concomitant initiation and propagation of these cracks), is then erroneous: rupture is likely in elastomer the consequence of the propagation and percolation of these cracks. As explained in rupture mechanics textbooks [8], [9], this propagation should occur when the energy needed to create crack surface is larger than the one stored in the material (and released/dissipated when crack propagates). Lake and Thomas [10] proposed that the energy needed to create the crack surface is equal to the one needed to

break the network chains at the crack front. Considering a monomodal and homogenous elastic network, they found a strain energy release rate proportional to $\nu^{-1/2}$. Equalling this value to the elastic energy released by the crack propagation in the crack tip vicinity, this could be a way to deduce a critical local deformation. The relation of the latter with a macroscopic critical deformation is however difficult to establish as the geometry/number of the pre-existing cracks (these one being likely submicrometric) is usually unknown. In addition, as said in the previous paragraph, elastomer networks are often not perfect, with dangling chains, sol fraction, and complex EAC length distribution, all things neglected by Lake and Thomas [5].

When an elastomer can crystallize during deformation, the understanding of its rupture behavior becomes even more difficult. Indeed, strain induced crystallization (SIC) leads both to strain hardening phenomenon and locally to chain relaxations, which have necessarily an impact on the rupture behavior. Ahagon et al. studying conventionally cross-linked NR, claimed that crystallization penalizes the elongation at break [7]. Nevertheless, they only based their interpretation on mechanical data and did not provide in situ WAXS data to support this assertion; moreover the large strain rate used in their study may have inhibited the crystallites nucleation and growth [11], [12]. Fortunately, we had the opportunity to study the same type of conventionally crosslinked materials, with different sulfur contents, i.e. different initial crosslinks densities. These materials have also been aged by thermo-oxidative ageing (TO) at 77°C. This ageing protocol leads to supplementary crosslinks and to negligible chain scissions [13]. Combining microstructural characterization techniques (MQ-NMR techniques, in-situ WAXS measurement and DSC analysis) the present paper aims at providing new insights not only on the specific behavior of these materials but also on the more general relationship between the microstructure of elastomer networks and their rupture properties.

2. EXPERIMENTAL

2.1 MATERIALS AND SAMPLES PROCESSING

The materials are unfilled natural rubber, obtained by gum vulcanization (Technically Specified Rubber TSR20) according to the recipe given in Table 1. The Sulfur/CBS ratios are above 1 in order to obtain “Conventional” system which contain mainly polysulfide bridges. These ratios are kept constant to ensure a same average length of the sulfur bridges, but in different concentrations in the processed materials. NR1.5_Eff with a Sulfur/CBS

below 1 is crosslinked with an "efficient" recipe leading to a network mainly crosslinked by monosulfides bridges. First, the gum is introduced in an internal mixer and sheared at 50 rpm for 2 min at 50 °C. The material is subsequently sheared at 70 rpm in an open mill for 5 minutes at 70 °C. Then the vulcanization ingredients are added and the so-formed mixture is sheared for 5 minutes at 50°C. Thin sample sheets (0.8 mm in thickness) are finally obtained by hot pressing at 30 bars under nitrogen flux, at 150°C for conventional system, and 170°C for efficient system. Cure times are estimated from the torque measurements performed with a Monsanto analyzer. They are defined as the time needed to obtain 98% of the maximum torque value (i.e t_{98} in min). Dumbbell-shaped samplesare machined with a 6 mm gauge length (l_0) and 0.8 mm thickness. The average density of the elastically active chain $\nu_{swelling}$ (EAC density) is estimated from swelling experiments and the Flory-Rehner equation [14]. These measurements are described in detail in our previous paper [13] . In order to avoid microstructural modification during the different mechanical tests, i.e. an uncontrolled Mullins effect (although this one is usually negligible in unfilled elastomer), the samples are successively stretched with the strain rate 1.1 10^{-1} s^{-1} four times just below the strain at break λ_{break} ($\lambda = \lambda_{break} - 0.2$) prior to mechanical characterization. It is worth mentioning that NR1.5 and NR1.5_Eff exhibit the same EAC density with different sulphur/CBS ratios.

Sample code	NR1.5	NR2	NR2.5	NR1.5_Eff
NR[a], phr[b]	100	100	100	100
6PPD[c], phr	3	3	3	3
Stearic Acid, phr	2	2	2	2
Zinc Oxide, phr	5	5	5	1.5
CBS[d], phr	0.5	0.75	1	1.9
Sulfur, phr	3	4.5	6	1.2
$\nu_{swelling}$ [e] (*10^{-4} mol.cm^{-3})	1.5	2	2.5	1.5
t_{98}, min	55	55	55	13

[a] Natural rubber TSR20.
[b] Parts by weight for hundred parts of rubber.
[c] N-(1.3-dimethylbutyl)-N'-phenyl-p-phenylenediamine.
[d] N-Cyclohexyl-2-benzothiazole sulfenamide.
[e] Average EAC density estimated from swelling measurements after vulcanization process (protocole described in reference 13).

Table 1 : Sample recipes and initial EAC density.

2.2 AGEING CONDITIONS

Aerobic ageing was performed on 0.8 mm thick samples in a convection oven at 77°C (350K). Such parameters were chosen as they enable to reproduce more realistically and over a reasonable duration, the ageing of rubber in some use conditions [15]. Special care was taken to ensure homogeneity of the degradation through the sample thickness (0.8 mm), i.e. to avoid any diffusion limited oxidation (DLO), by following the procedure of reference [16]. When not tested, all the samples are then stored at 7 °C to avoid any degradation. When tested, they are first maintained at 60°C during 5 min to avoid any presence of crystallites.

2.3 INSTRUMENTS

2.3.1 THERMAL CRYSTALLIZATION

Samples of 10 mg were cooled in a freezer (at -31°C) during one year. This temperature has been chosen to favor the crystal nucleation. It is slightly below -25°C which is the temperature needed to obtain the highest crystallization rate with efficiently crosslinked NR [17], [12], [18] and uncrosslinked NR [18], [19] (cf. Fig S1 in SI). This difference is ascribed to the more difficult nucleation of crystallites for these materials which are more crosslinked and in which polymer chains are likely more functionalized by sulfide pendant groups [13], [20]. After thermal crystallization, samples are then transferred in a Perkin–Elmer Pyris Diamond calorimeter (DSC), using a cryo-transfer specimen holder. They are pre-cooled in the DSC cell at -40°C, followed by an isothermal step at –50°C for 2 min. They are then heated at 10°C.min^{-1} up to 30°C in order to melt all crystallites.

2.3.2 TENSILE TESTS

Tensile tests were performed with an MTS device equipped with a temperature-controlled chamber. Digital image correlation (DIC) was used to obtain the real local strain in the zone of interest. Experiments were conducted at 25°C with a true strain rate of $4.2*10^{-3}$ s^{-1} on Dumbbell-shaped samples, with a 6 mm gauge length

(l_0) and 0.8 mm thickness. For reproducibility, three samples were tested. Given the good reproducibility, only one stress-strain curve is reported. Treloar model predicts for elastomer without strain hardening [21] :

$$\sigma_{nom} = \frac{E}{3}(\lambda - \frac{1}{\lambda^2}) \quad (1)$$

Where σ_{nom} is the nominal stress, E the Young modulus and λ the stretch ratio l/l_0, where $l_0(l)$ is the initial (elongated) length of the sample. To estimate E, the curve were fitted between λ = 1 and λ = 1.3. The EAC density, within the affine assumption, is related to the Young modulus through this equation:

$$\nu_{mecha} = \frac{E}{3RT} \quad (2)$$

Where R corresponds to the perfect gas constant (8.314 J.mol^{-1}.K^{-1}) and T the testing temperature.

2.3.3 IN-SITU WAXS

The in-situ WAXS experiments are carried out on the D2AM beamline of the European Synchrotron Radiation Facility (ESRF). The X-Ray wavelength is 1.54 Å and the beam size is 300 µm × 200 µm. A homemade stretching machine allowing the symmetric deformation of the sample is used to probe by X-Ray the same sample position during stretching at 4.2*10^{-3} s^{-1}. This strain rate is a compromise between the crystallization kinetic (when too rapid, the strain induced crystallization is lowered at a given strain) and the acquisition time (the experiments must not be too long for practical reason). This strain rate is chosen in the "quasi-static" range, as shown and discussed in reference [11]. The two-dimensional (2D) WAXS patterns are recorded every 15 seconds ($\Delta\lambda \approx 6\%$ between two spectra). The background is properly measured without sample and can be subtracted to the total intensity scattered in the presence of the rubber sample. The corrected scattering intensity is finally corrected, taking into account the continuous variation of the sample thickness and possible incident beam fluctuations. Each scattering pattern is integrated azimuthally. The deconvolution of the curve $I = f(2\theta)$ shown in Fig. S2 enables the measurement of the intensity at the peak top and the width at half height of each crystalline peak, and of the intensity at the peak top of the amorphous phase. The volume fraction of crystallinity named χ_v is then calculated using the Mitchell approach [22] :

$$\chi_v\,(\%) = \frac{I_{a0} - I_{a\lambda}}{I_{a0}} \quad (3)$$

Where I_{a0} and $I_{a\lambda}$ are the intensity of the amorphous phase at the peak top in the unstretched and stretched state respectively. The average crystallite sizes L_{hkl} in the direction normal to the (hkl) planes are estimated from the Scherrer equation:

$$L_{hkl} = \frac{K\lambda_w}{\beta\cos(\theta)} \quad (4)$$

Where λ_w is the wavelength and θ the Bragg angle. As shown in Fig. S2 in SI, each crystalline peak can be fitted with a Lorentzian function in which the half width at the half height is β. According to the parameters chosen for the simulation of the experimental peak, the value selected for K is 0.64 [17].

2.3.4 MQ-NMR EXPERIMENTS [23]

Experiments were carried out on a Bruker minispec mq20 spectrometer operating at 0.5T with 90 pulses of 3 µs length and dead time of 11 µs. The temperature was fixed at 40 °C. The data analysis involves a normalization procedure using two sets of experimental data, the DQ buildup (I_{DQ}) and reference decay (I_{ref}) curves. Both were measured as a function of the double quantum evolution time (τ_{DQ}) which represents the variable duration of the pulse sequence (cf. Fig. 1a) [24]. The sum of both components, $I_{\Sigma MQ} = I_{DQ} + I_{ref,}$ corresponds to the signal from dipolar coupled network segments and the signal for uncoupled, i.e. mobile networks defects such as dangling chains, loops and sol chains.

The individual fractions of network are characterized by different relaxation behavior: coupled segments relax faster while the signal for uncoupled segments shows a progressive exponential decay (T_{B2} in Eq. 5). This difference can be amplified by plotting $I_{ref} - I_{DQ}$ on Fig. 1b. As a consequence, it is necessary to identify and subtract the exponential long-time contribution (i.e, the non-coupled fraction of polymer chains associated with the last term of the Eq. 5 and fitted in Fig. 1b) to the total signal $I_{\Sigma MQ}$:

$$I_{\Sigma MQ} = I_{DQ} + I_{ref} - Be^{\frac{-2\tau_{DQ}}{T_{B2}}} \quad (5)$$

Where B is the noncoupled fraction of polymer chains and T_{B2} is the slow exponential decay factor of elastically non-active defects. After the identification and subtraction of the contribution of non-elastic networks defects, structural information about the elastomer network can be obtained independently on relaxation effects by normalizing the signal from dipolar coupled network segments I_{DQ} by the total signal $I_{\Sigma MQ}$:

$$I_{nDQ} = \frac{I_{DQ}}{I_{\Sigma MQ}} \tag{6}$$

The signal I_{nDQ} is only related to the network structure and is independent of any temperature-dependent relaxation effect. The latter equation depends on the residual dipolar couplings D_{res} which reflects the anisotropy arising from cross-links and topological constraints [25]. The proper analysis of I_{nDQ} plotted in Fig. 1c provides information about the residual dipolar couplings D_{res} and their distribution assuming that each monomer can be characterized by a single D_{res} value [26].

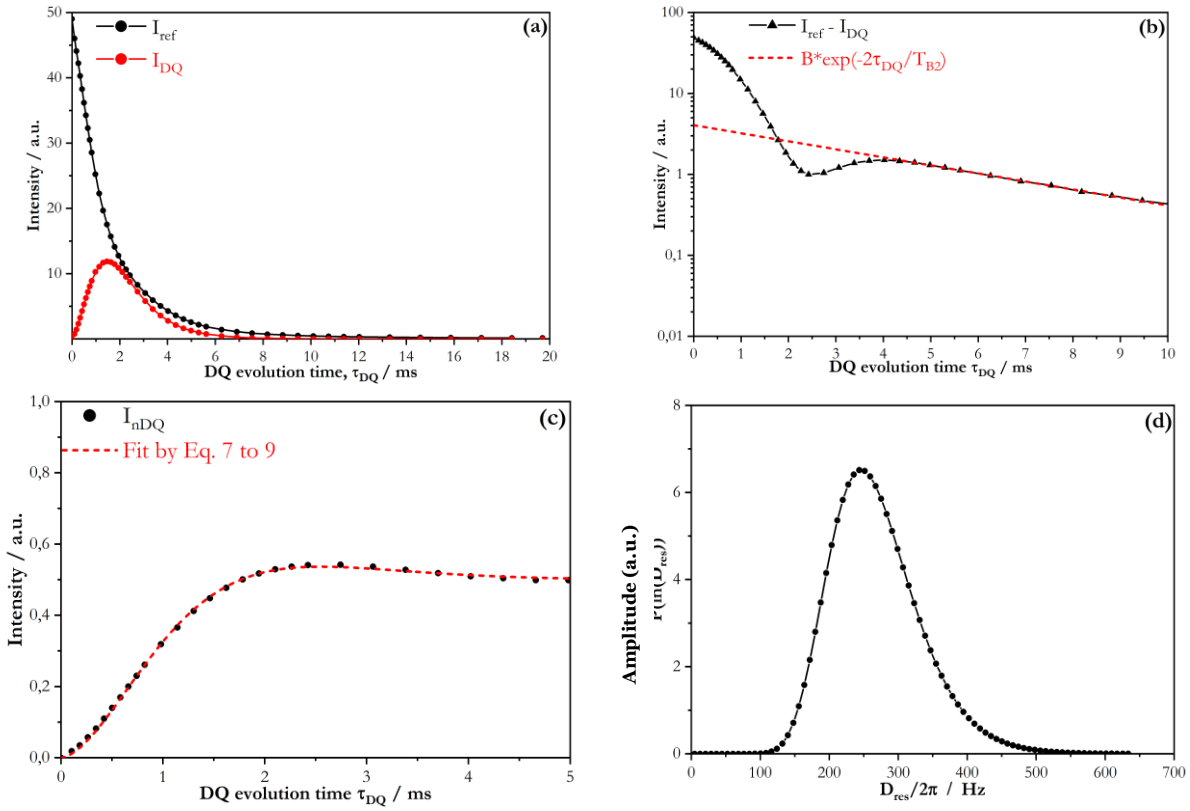

Fig. 1 : Regularization procedure and data analysis for NR2.5 sample. (a) The raw build-up (I_{DQ}) and reference decay (I_{ref}) data are represented as a function of the double quantum evolution time τ_{DQ} (b) The difference $I_{ref} - I_{DQ}$ is used to identify the more slowly relaxing non-elastic defect fraction (c) The latter has to be subtracted to obtain a proper point-by-point normalization of the DQ intensity I_{nDQ} as a function of τ_{DQ} (d) The corresponding distribution using Eq. 9.

Let us now consider the shape of the normalized I_{nDQ} build-up curve in Fig. 1c. It displays a continuous increase as τ_{DQ} is raised up to about 2.5 ms and above this value, a plateau value at 0.5 is observed. As discussed in [27], the normalized build-up curve may be expressed as:

$$I_{nDQ}(\tau_{DQ}) = \int P(\ln\left(\frac{D_{res}}{2\pi}\right) \times I_{nDQ}\left(\tau_{DQ}, \frac{D_{res}}{2\pi}\right) d\ln\left(\frac{D_{res}}{2\pi}\right) \quad (7)$$

In order to be more accurate with this analysis, an improved function, the so called "Tikhonov regularization", has been developed [28] and has been used in this study to fit properly $I_{nDQ}(\tau_{DQ}, \frac{D_{res}}{2\pi})$ data :

$$I_{nDQ}\left(\tau_{DQ}, \frac{D_{res}}{2\pi}\right) = 0.5(1 - e^{-\left(0.378\frac{D_{res}}{2\pi}2\pi\,\tau_{DQ}\right)^{1.5}} \times \cos\left(0.583\frac{D_{res}}{2\pi}2\pi\,\tau_{DQ}\right)) \quad (8)$$

A satisfactorily fit of the $I_{nDQ}(\tau_{DQ})$ evolution reported in Fig. 1c was obtained by means of the following distribution $P\left(\ln\left(\frac{D_{res}}{2\pi}\right)\right)$:

$$P\left(\ln\left(\frac{D_{res}}{2\pi}\right)\right) = \frac{1}{\sigma_{ln}\sqrt{2\pi}} \times e^{-\frac{\left(\ln\left(\frac{D_{res}}{2\pi}\right) - \ln(D_{med})\right)^2}{2\sigma_{ln}^2}} \quad (9)$$

i.e., a Gaussian distribution of $\ln\left(\frac{D_{res}}{2\pi}\right)$ with the parameters D_{med} = 261 Hz and σ_{ln} = 0.24 for NR2.5. This distribution is strictly equivalent to a log-normal distribution of $\frac{D_{res}}{2\pi}$ with the parameters ($\ln(D_{med})$, σ_{ln}). We use

here the procedure described by MQ-NMR specialists [24] [27]. Of course such distribution ignores the possible existence of bimodality, or multimodality in the EAC lengths distribution. Nevertheless, we do not have enough information to estimate the relevance of the use of several distributions, either to evaluate their parameters. A log-normal distribution appears to be appropriate when a large distribution of EAC lengths is expected.

The log-normal distribution obtained for NR2.5 is plotted in Fig. 1d. From these parameters, the molecular weight between constraints, M_c (kg.mol^{-1}), can be estimated for NR samples by:

$$M_c^{(NR)} \Leftrightarrow \frac{617\ \text{Hz}}{\langle \frac{D_{res}}{2\pi} \rangle} \tag{10}$$

Where $\langle \frac{D_{res}}{2\pi} \rangle$ for a log-normal distribution is related to D_{med} through:

$$\langle \frac{D_{res}}{2\pi} \rangle = D_{med} * e^{\frac{\sigma_{ln}^2}{2}} \tag{11}$$

There is some degree of approximation in the prefactor 617 Hz obtained by modeling proton-proton interactions in numerical simulations [26]. Nevertheless, this formula has been widely used in literature [29], [30]. Finally, the EAC density ν_{NMR}, can be deduced from:

$$\nu_{NMR} = \frac{\rho}{M_c} \tag{12}$$

Where ρ is equal to 0.92 g.cm^{-3} for natural rubber.

3. RESULTS

3.1 THERMAL CRYSTALLIZATION OF UNDEFORMED SAMPLES AT -31°C

Sample subject to cold crystallization should be also subject to strain induced crystallization. Thus, a study by DSC of their cold crystallization can provide information on the ability of the materials to cristallize under strain. Thus, heating curves and corresponding crystal weight fraction in % of non-aged and aged NR after 12 months spent at -31°C are presented in SI (cf. Fig. S3). NR1.5 with the lowest average network chain density exhibits multiple melting peaks, which is a classical feature for the cold crystallization of unvulcanized or weakly vulcanized natural rubber [18], [19], [31]. The lowest melting peak is generally ascribed to less stable β lamellae

and the highest to more stable α lamellae [19], [31]. The proportion of α lamellae decreases with the increase of the EAC density. Within the assumption of a lamellar crystallization, a rapid calculation using the Gibbs Thomson equation enables to estimate the thickness of the crystallites whose melting temperature would correspond to the α and β peak temperature: in the case of unaged NR1.5, with ΔH_f of 6,1 10^7 $J.m^{-3}$ [31], a melting temperature T_f of 35,5 °C [32] and a folding surface energy σ_e of 0,02 $J.m^{-2}$ for the α peak and 0,04 $J.m^{-2}$ for the β peak [33], the deduced distances are 47 Å and 77 Å, which are in the range of the L_{002} dimension of the cristallites induced by strain. Crystal weight fraction is finally measured taking into account the contribution of both α and β lamellae, and using a melting enthalpy of 67.3 $J.g^{-1}$, i.e. the value of the melting enthalpy of a perfect natural rubber crystal [18].

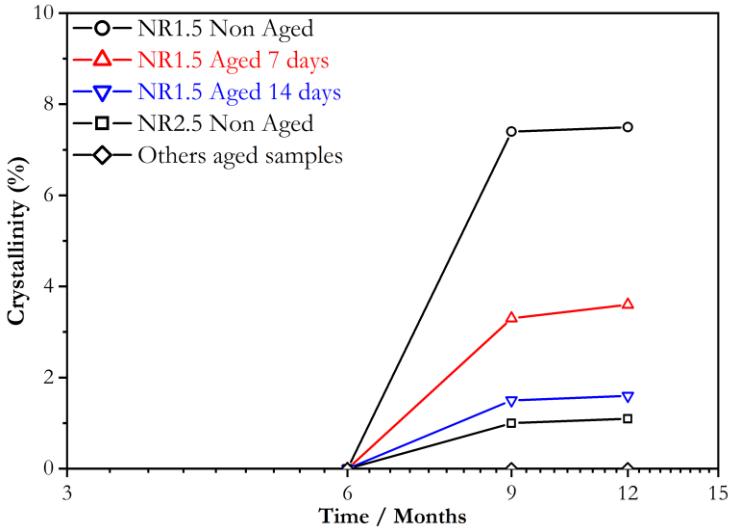

Fig. 2 : Crystallinity versus time a -31°C for non-aged and aged NR after 6, 9 and 12 months – *Lines are plotted as a guide for the eyes*

The crystallinity values measured at 6, 9 and 12 months are plotted on Fig. 2. It shows that the 12 months value is close to the maximum one and can be considered as the maximum crystallinity that can be reached in the material by cold crystallization. This value is the highest for NR1.5 and then rapidly decreases for higher values of ν. For the most degraded materials (NR1.5 aged 21 days and aged NR2.5) for which the EAC density is higher, no cold crystallization was observed. Note that, in the case of NR1.5_Eff, which exhibits the same EAC density as NR1.5, the maximum crystallinity obtained by DSC is around 4 times higher (cf. Fig. S1 in SI). Two

explanations can be proposed for this difference: a different distribution of the active chain length, and the presence of more grafted species on the NR1.5 chains which can hinder the crystallization [13].

3.2 CONSEQUENCES OF AGEING ON MECHANICALS PROPERTIES

The tensile stress-stretch ratio curves obtained at room temperature, for aged and non-aged samples are reported in Fig. 3. We have plotted on Fig. 4, ν_{mecha} deduced from these tensile tests and Eq. 2, as a function of $\nu_{swelling}$, assuming an affine model in both cases. $\nu_{swelling}$ are calculated with a constant functionality of 4, and with the corrected χ parameter deduced from swelling experiments with two different good solvents (toluene & cyclohexane). All the details about swelling measurements are described in a previous publication [13]. The relationship between data from swelling and from mechanical tests is quasi-linear, with a slope close to 1. This is expected as the sol fraction of all the samples is low, and around 4-5 % (cf. Fig. S4 in SI). Thus, swelling measurement (with two solvents) appears here as a very good technique to estimate the evolution of the modulus of our aged natural rubbers, even if their EAC density is significantly changed. This is of practical interest since this technique requires much less material.

Prior to ageing treatment, cf. Fig.3, NR1.5 had the lowest EAC density, resulting in a modulus of 1.1 MPa, while NR2 and NR2.5 had higher modulus, of 1.4 MPa and 1.5 MPa respectively. All the natural rubber samples, processed according to our recipe and processing conditions, showed an increase in the modulus and a decrease in stress and stretch ratio at break after thermo-oxidative ageing at 77°C since it mainly leads to supplementary crosslinking [13]. For NR1.5, σ_{break} decreases from 3.6 ± 0.2 down to 1.8 ± 0.2 MPa after 21 days, for NR2 from 3.9 ± 0.2 MPa down to 1.6 ± 0.2 MPa, and for NR2.5 from 3.6 ± 0.2 MPa down to 1.6 ± 0.2 MPa.

λ_{break} is plotted versus the ageing time in Fig. 5 for all the materials. Its value decreases rapidly for the first ageing durations and then becomes relatively constant for larger ageing time, except for NR1.5 where there is no noticeable stabilization (it is likely that the experiment did not last long enough to observe it). The evolution observed for NR2.5 and NR2 suggests that the most degraded material may break before any strain induced crystallization can occur. Hence, the materials have been studied by WAXS measurements.

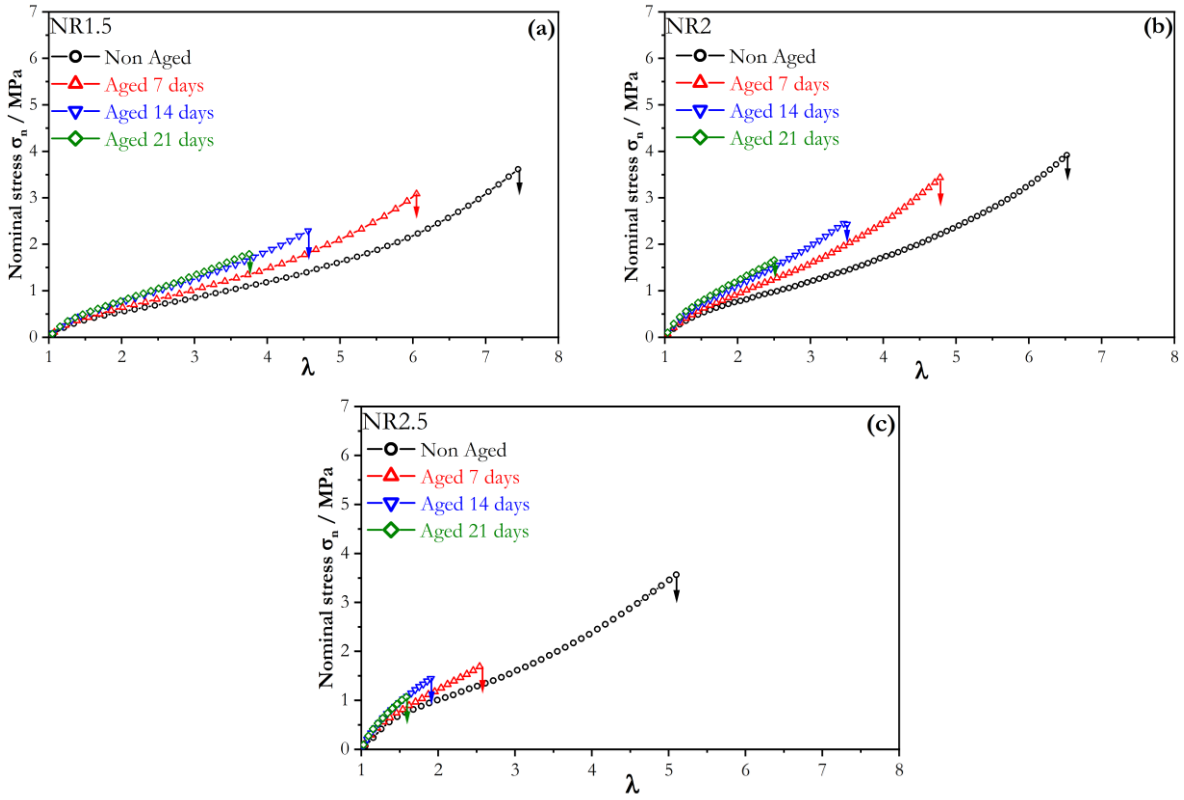

Fig. 3 : Stress-Stretch ratio curves obtained at 25°C, as a function of the ageing time and the sample : (a) NR1.5 (b) NR2 (c) NR2.5

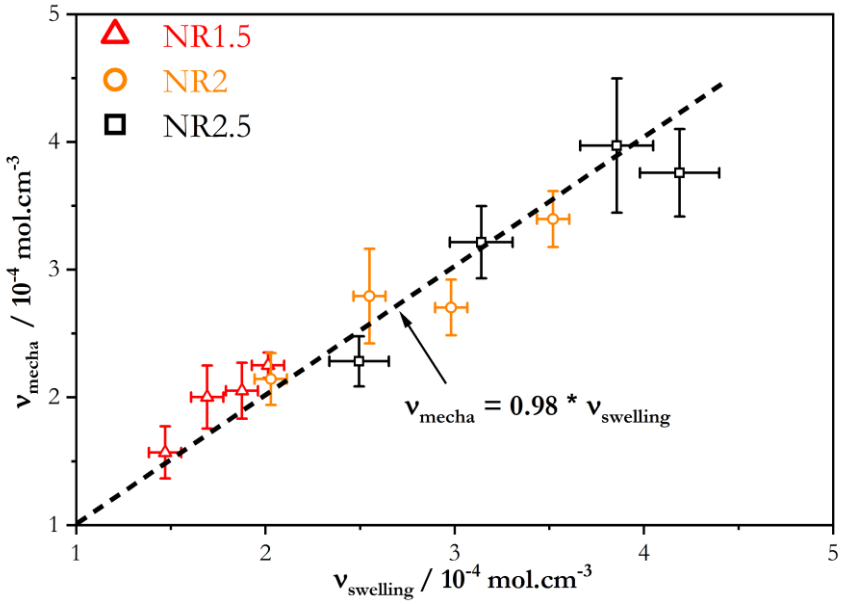

Fig. 4 : ν_{mecha} as a function of $\nu_{swelling}$ for all the samples

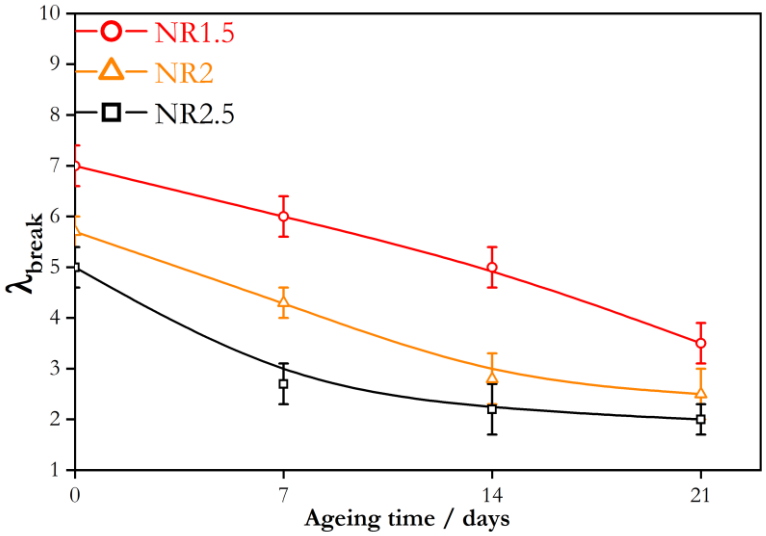

Fig. 5 : λ_{break} as a function of ageing time at 77°C for NR1.5, NR2 and NR2.5 - *Lines are plotted as a guide for the eyes*

3.3 STRAIN-INDUCED CRYSTALLIZATION ANALYSIS

Vulcanized samples were stretched from the underformed state up to elongation at break, at $4.2*10^{-3}$ s^{-1} and 25°C. Among all the samples tested, only the samples breaking at λ above 4 displayed strain induced crystallization. Thus, when aged 21 days, NR1.5 breaks before the onset of crystallization. The crystal volume fraction χ_v calculated by the Mitchell approach is plotted as a function of λ in Fig. 6a for NR1.5 and Fig. 6b for NR2.5 (Unfortunately, no measures were performed on NR2). The stretching ratio at crystallization onset λ_c is around 4 and seems independent of the EAC density. This value is typically found in literature for vulcanized rubbers [12], [33]–[35]. Prior to degradation, NR1.5 and NR2.5 exhibit at λ_{break} a crystal volume fraction of 10% and 5%, respectively. The crystallization rate is not correlated with $\nu_{swelling}$ as it is roughly the same for non-aged NR1.5 and NR2.5 although they do not have the same EAC density. For NR1.5, which is the only material for which we observe SIC for the different ageing times, this rate increases with the ageing time. In spite of this, due to the decrease of λ_{break} with ageing, its maximum crystal volume fraction decreases with the increase of the ageing time.

Sample code	EAC density (10^{-4} mol.cm^{-3})	χ_v (%)	L_{200} (Å)	L_{120} (Å)	L_{002} (Å)

NR1.5_NonAged	1.5	2.9 ± 0.5	97 ± 1	35 ± 1	62 ± 1
NR1.5_A7	1.7	3.6 ± 0.5	80 ± 1	27 ± 1	55 ± 1
NR1.5_A14	1.9	5.4 ± 0.5	65 ± 1	17 ± 1	47 ± 1
NR2.5_NonAged	2.5	3.5 ± 0.5	60 ± 1	18 ± 1	45 ± 1

Table 2 : Characteristics of the crystal phase measured at λ = 5.

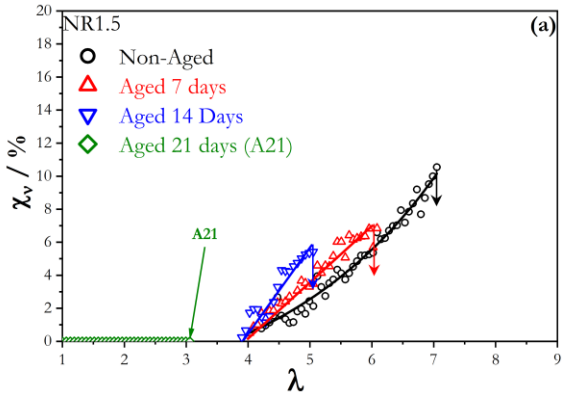

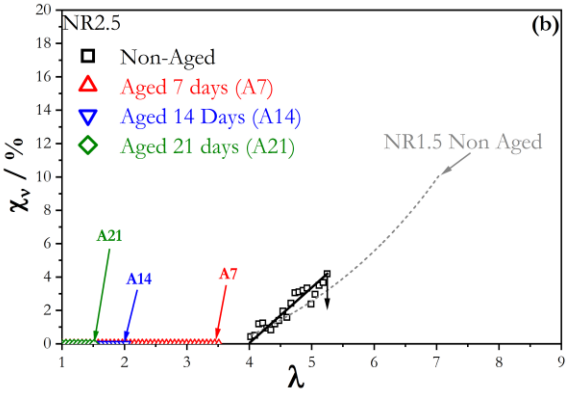

Fig. 6 : χ as a function of λ at room temperature and slow strain rate ($4.2*10^{-3}$ s^{-1}) at different ageing time for NR1.5 (a) and NR2.5 (b). *Lines are plotted as a guide for the eyes*

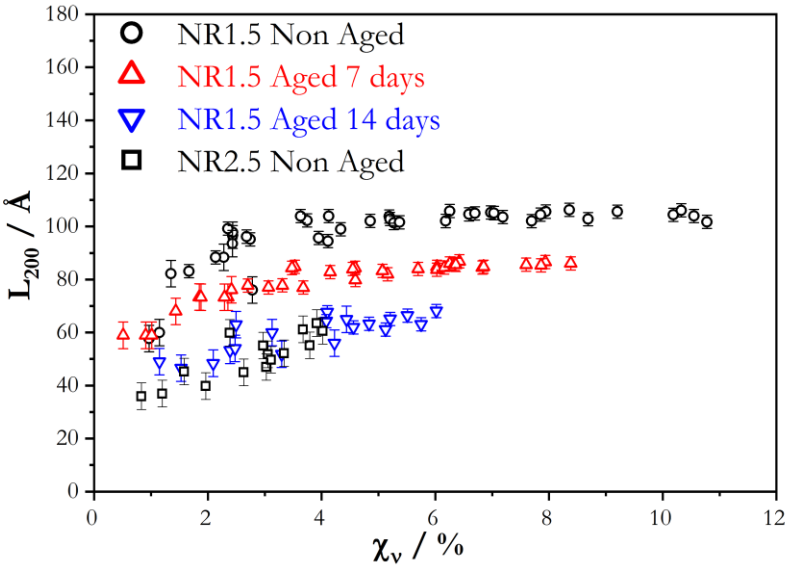

Fig. 7 : L_{200} as a function of χ (%) for samples able to crystallize under strain

L_{200} is plotted as a function of χ_v for samples able to crystallize when strained, in Fig. 7. L_{120} is roughly equal to 1/3 L_{200} and L_{002} is roughly constant as previously reported in literature [12], [33]–[35]. The increase of L_{200} with λ, and thus with χ_v, is in agreement with studies on filled and unfilled rubbers [34], [36] but in disagreement with other works that report no evolution [37] or a decrease with the stretch ratio [38]. These discrepancies should come from the difficulty to accurately estimate the width at mid-height of the crystalline peak (β in Eq. 4) when the diffracted intensity is weak. To overcome this limitation, our strategy consisted in the deconvolution of the WAXS patterns from the highest to the lowest level of crystallinity.

Some characteristics of the crystal phase are reported in Table 2 for each sample for λ = 5. Similarly to previous results [12], [34], the higher the crosslink density, the lower the crystallites dimensions. Such behavior is explained by the limitation of crystallite growth by topological constraints created by the more numerous crosslinks. The evolution of the crystallite size and of the crystallite number should therefore be the consequences of both spatial and length distribution of the EAC as previously discussed in reference [33] A quite

similar $\chi_v(\lambda)$ curve is found for unaged NR1.5 and unaged NR2.5 (except that it is more rapidly stopped for NR2.5, cf. Fig. 6b); thus, at a given crystalline volume fraction, the crystallite populations in NR2.5 are much more numerous and smaller than in NR1.5. Moreover, thermo-oxidation of NR1.5 leads for a given λ to a decrease of the crystallites sizes while the crystal volume fraction increases, meaning that more numerous and smaller crystallites are formed during stretching. Such comment cannot be done for aged NR2.5, since after 7 days of thermo-oxidative ageing, it breaks before showing any strain induced crystallization. All these results can be related to the elastomer network structure which was characterized by MQ NRM.

3.4 MQ NMR EXPERIMENTS

Chain length distributions can be characterised by MQ-NMR [29], [30], [39] which also provides information about the proportion of noncoupled network defects. The fraction of non-elastic networks defects is quantified from the coefficient B in Eq. 5 and reported in Table S1 in SI. All non-aged networks contain approximatively 3% of non-elastic defects, which is a quite low value, but is expected here as the samples are made from high molecular weight chains, with a relatively high crosslink density (M_c < 6200 g.mol^{-1}). This value is also consistent with the low Soluble Fraction previously reported.

The normalized DQ buildup curves are shown in Fig. 8a. Its increase is more rapid with the most crosslinked samples. The corresponding distributions of D_{res} obtained by regularization fitting procedure are shown in Fig. 8b**.** Prior to ageing, distribution of D_{res} are already different between the three samples, particularly for non-aged NR2.5, for which the shape of the peak suggests a larger distribution of the EAC length with populations with much smaller contour length than in NR2 and NR1.5.

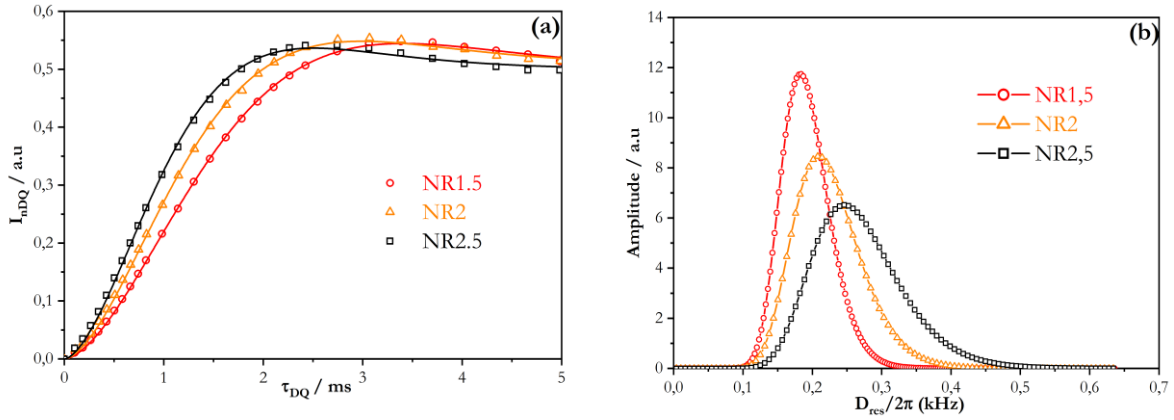

Fig. 8 : (a) Normalized proton DQ-NMR buildup curves for the different non-aged samples (b) Corresponding D_{res} distributions

Evolution of EAC densities after ageing can be estimated from the average value of D_{res} (cf. Fig. 9) and calculated via the Eq. 11. It is plotted as a function of $v_{swelling}$ in Fig. 10. A linear relationship is found with a slope of 0,874, i.e. close to 1. Even if expected, this slope is different from the one around 2 found in literature [30], [40]. Note that in these references, a Gaussian distribution was used for D_{res} whereas we used a lognormal one. However, this cannot explain such discrepancy, for which we do not have clear explanation.

More interestingly, the fitting line has non-zero y-intercept. It is related to the different time scales which are probed in each experiment: in NMR, the response involves chains segments dynamics on a time scale of the order of 10^{-4} s. That means that it also involves all the topological constraints created on each chain by its surrounding (often summarized by the concept of "free entanglements"), whereas equilibrium swelling experiments only involves the elastically active chains created by the chemical crosslinks or the trapped entanglements. Thus, the measured EAC densities values at non-zero y-intercept may provide an estimate of the molecular weight between entanglements (M_e) which is found here equal to ca. 5800 g.mol^{-1}. This value is quite consistent with published values from rheological experiments on 1,4-polyisoprene (≈ 6200 g.mol^{-1}) [41].

The standard deviation σ_{ln} of the Log Normal distribution defined in Eq. 9 is plotted as a function of the average EAC density in Fig. 11 for the different samples. Prior to ageing, the less distributed network is obtained for the

less sulfured rubber, NR1.5 (σ_{ln} around 0.18). Thermo-oxidative ageing leads to the enlargement of the distribution which becomes less and less symmetric, as evidenced by the increase of σ_{ln}. The more initially crosslinked the sample, the more important the enlargement of this distribution. These results are consistent with previous thermoporosimetry experiments [13].

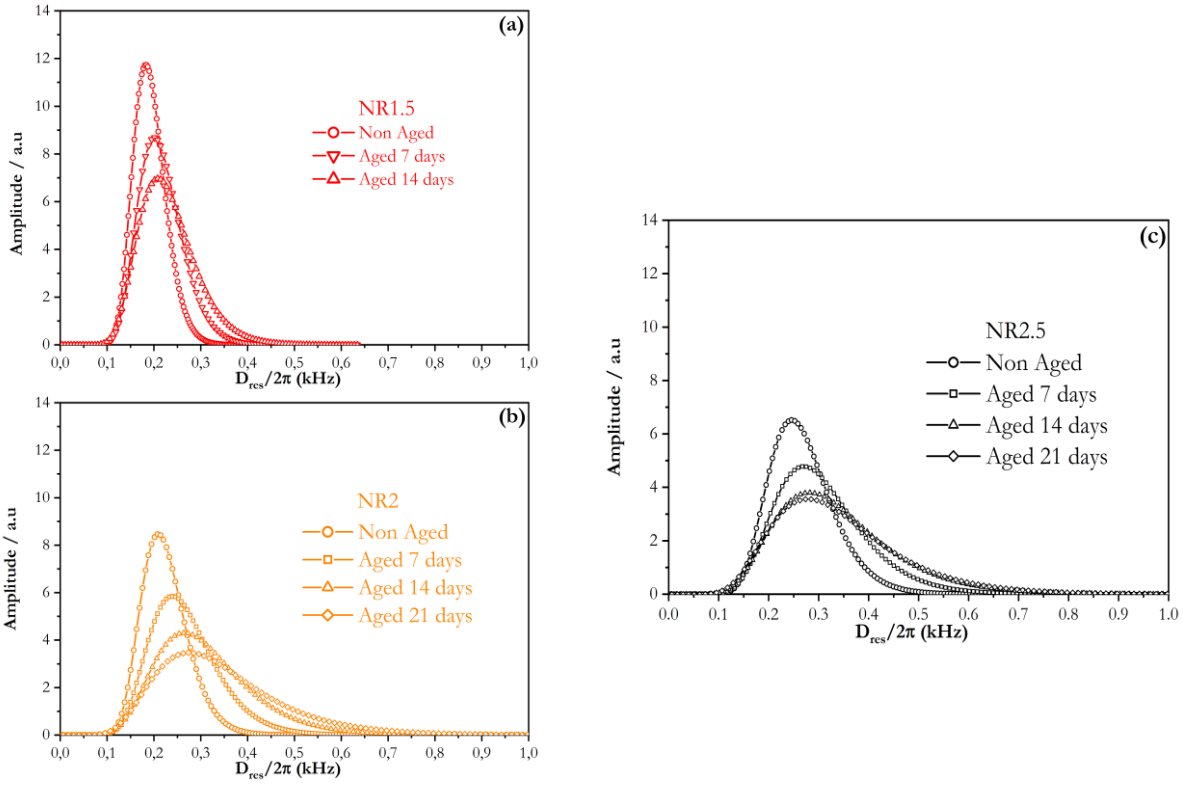

Fig. 9 : Normalized proton DQ-NMR buildup curves for the different aged and non-aged (a) NR1.5 (b) NR2, (c) NR2.5.

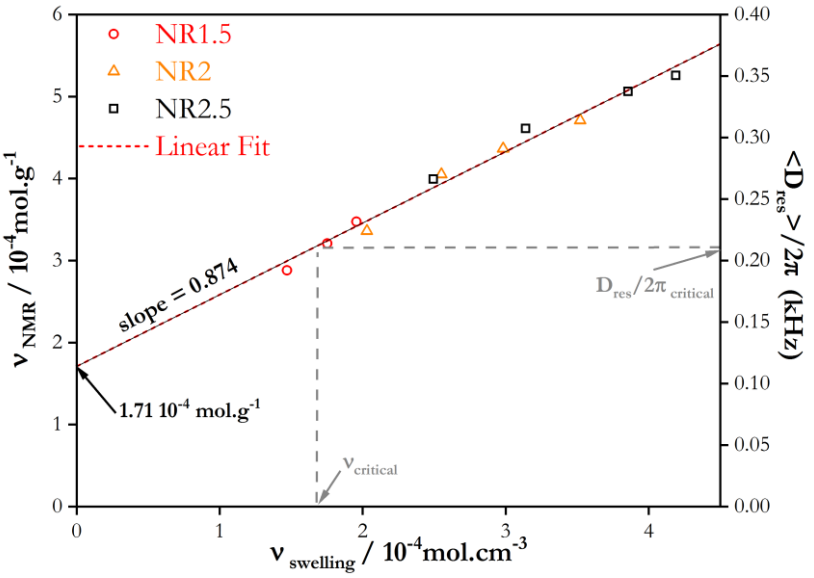

Fig. 10 : Average EAC densities and D_{res} estimated by MQ-NMR as a function of $\nu_{swelling}$ (Data from [13]) assuming an affine model – Red dashed line is a linear fit with the corresponding slope. Grey dashed lines linked the value of $\nu_{critical}$ and $D_{res\ critical}$ (discussed later)

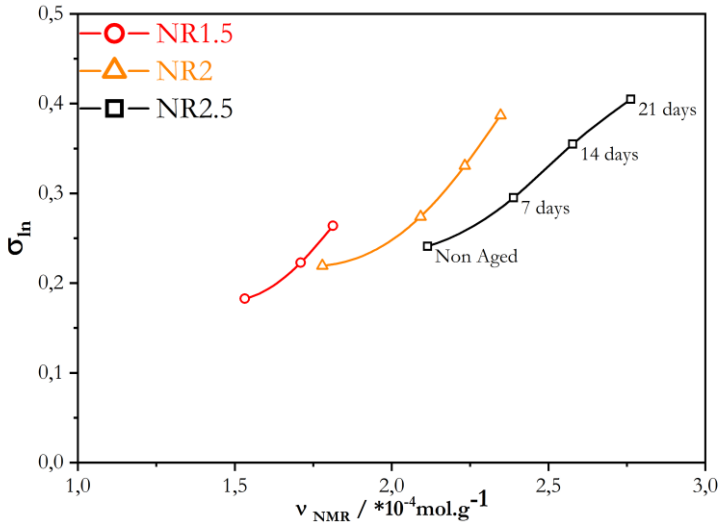

Fig. 11 : Distribution width (σ_{ln}) as a function of the average EAC density ν_{NMR} - *Lines are plotted as a guide for the eyes*

4. DISCUSSIONS

As reported in reference [13]**,** EAC density of the studied material obtained after processing (55 minutes at 150°C) increases with the initial concentration of sulfur S_8. This latter is not totally consumed in the crosslinking

reaction during vulcanization process, even if the curing time has been chosen to optimise the initial properties of the materials. Moreover, long polysulfidic bridges are formed and polysulfidic groups are grafted on the NR backbone. They are therefore all available for supplementary crosslinking reactions occurring during thermo-oxidative ageing at 77°C. They are more important for NR2.5 due to a higher concentration of residual sulfur content and polysulfidic cyclic groups along the polymer chains. Such evolution modifies the material mechanical properties (cf. Fig. 3), in particular the rupture ones (cf. Fig. 5). The observed decrease in stretch ratio at break with increasing ageing time is consistent with the increase of the EAC density, since λ_{break} should be related to the maximum extensibility of the Elastically Active Chains (this one decreasing with their initial contour length). Following this approach, theorized by Kuhn, λ_{break} should depend on the inverse square root of the EAC density [1] :

$$\lambda_{break} \propto K.\nu^{-1/2} \quad (12)$$

λ_{break} is therefore plotted as a function of $\nu_{swelling}$ in log scale in Fig. 12.

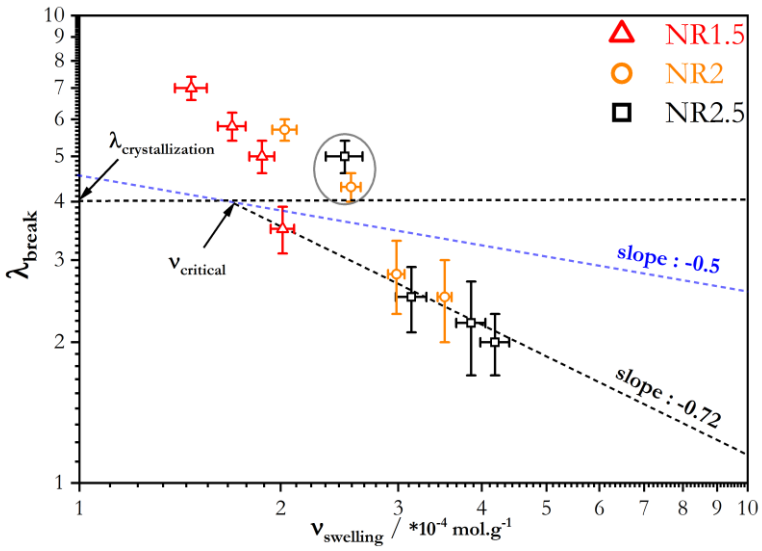

Fig. 12 : Stretch ratio at break as a function of $\nu_{swelling}$ for NR1.5, NR2 and NR2.5 after thermo-oxidative ageing. Measurements performed at 25°C.

This plot displays two domains separated by the usual stretch ratio at the onset of crystallization λ_c = 4. For $\lambda < \lambda_c$, a power law is indeed found, with a negative exponent around -0.72. This one is different from the -0.5

predicted by Kuhn. It is however close to the one found by Ahagon (exponent -0.75) with filled NR conventionally crosslinked or by Akagi with hydrogels (exponent -0.65) [36]. It is worth mentioning that Ahagon performed tensile test with a crosshead speed of 8.33 mm.s^{-1} [7] which suggests that the strain rate used (around 0.4 .s^{-1}) is much larger than the one we used (0.004 s^{-1}). With this rate, the strain induced crystallization in his materials is unlikely, and in any case, less important.

The -0,75 exponent may find an explanation if one considers crack propagation mechanisms. As recalled in the introduction, this propagation is possible when the energy it releases is larger than the one needed to create the supplementary crack surface. Lake and Thomas predicting that this one is proportional to $\nu^{-1/2}$, it could be tempting to equal it to the macroscopic elastic energy at λ_{break} divided by the sample section. At large stretch ratio, for an elastomer without strain hardening and that can be described by equation 1, this surface energy is roughly proportional to $E(\lambda_{break})^2$ time the sample length at break. E being proportional to ν, one find indeed λ_{break} proportional to $\nu^{-0,75}$. Note however that, very paradoxically, the materials which enables to find the -0,75 exponent are the ones for which λ_{break} is small and therefore for which the approximation of the strain energy as $E(\lambda_{break})^2$ is wrong (especially for the NR2.5 materials). Thus, this explanation must be taken with great caution and is not really satisfactory. One may also use the Greensmith formula which predicts a strain release energy roughly proportional to $\frac{W(\lambda)a}{\sqrt{\lambda}}$, where a is the initial length of the pre-existing cracks in the material. Using the same approximation for the strain energy $E(\lambda_{break})^2$ and the Lake and Thomas prediction, the -0,75 power law dependence implies that the initial crack length should depend on $\nu^{\frac{3}{4}}$. To the author's knowledge, there is no reason for such dependence, which looks fortuitous.

The DSC results (cf. Fig. 2) show that after 12 months at -31°C, thermal crystallization only occurs in NR1.5 non aged, aged 7 days or 14 days, and non-aged NR2.5. In spite of the lack of results for NR2, these findings suggest that the proportionality between $\ln(\lambda_{break})$ and ν is only verified for materials which cannot thermally crystallize. For these materials, the crosslink density may be too large after ageing to enable the crystallites nucleation. Conversely, for samples which can deform above λ_c = 4, stretch ratio at break is higher than the one predicted by the drawn line in Fig. 12. In that case, WAXS experiments have shown that these samples can

crystallize (cf. Fig. 6). This phenomenon seems to act as a reinforcement mechanism and improves the material rupture properties.

It is noteworthy that the extrapolation of the ($\lambda_{break} = \nu_{swelling}{}^{-0,72}$) curve cut the horizontal line $\lambda_{break} = 4$ at $\nu_{swelling}$, around 1.7*10^{-4} mol.cm^{-3} (so called hereafter $\nu_{critical}$), i.e. for a M_c value of 5400 g.mol^{-1}. Such value corresponds approximately to the molecular weight between physical entanglements in natural rubber [41] and is remarkably close the one previously deduced from Fig. 10. This value was already found to be a key parameter for the crystallization rate in natural rubber [34], and the results of Candau also suggests that the EAC with this molecular weight are at the origin of the most numerous crystallites population appearing during stretching [33].

Given their EAC density, non-aged NR2.5 and NR2 aged 7 days (highlighted by a grey circle in Fig. 12), one would have expected that they follow the same trend as the samples whose $\nu_{swelling}$ is above 1.7*10^{-4} mol.cm^{-3}. However, their rupture occurs beyond the onset of crystallization $\lambda_c = 4$. This result could be explained by their chain length distributions, which may contain a sufficient fraction of EAC long enough to crystallize before breaking. In other words, we suggest that in these samples, in spite of their high crosslink density, weakly crosslinked domains or phases ($\nu < \nu_{critical}$) exist which can reach λ_c and therefore crystallize. This is supported by the fact that, conversely to NR1.5 aged 21 days, the non-aged NR2.5 is indeed able to crystallize at -31°C (cf. Fig. 2).

Although the D_{res} distribution is not a quantitative representation of EAC distributions (since it is actually the result of the convolution of this distribution with the one related to the coupled segments dynamics in each EAC), it enables an insightful semi-quantitative comparison of the EAC length distribution of the different samples. A $D_{res\,critical}$ can be deduced from the previous $\nu_{critical}$ value by the use of Fig. 10. One reads on this figure the value 0.21. Using the distributions presented in Fig. 9, we propose to calculate a parameter from the D_{res} distribution:

$$P(\%) = \frac{\text{Area for } D_{res} < D_{res\,critical}}{\text{Total Area}} \tag{13}$$

A schematic description of its calculation is described in SI (cf. Fig. S5). The parameter P(%), since it is the

result of both distribution width and density of the EAC seems, a pertinent parameters. Indeed, it qualitatively provides an estimate of the proportion P(%) of chains, which can crystallize under strain. Elongation at break of all the samples is plotted as a function of P(%) in Fig. 13. The maximal crystal volume fraction χ (in %) is also reported. The plot displays two different regimes. For P(%) $\geq$ 17%, natural rubber is able to reach the onset of crystallization λ_c = 4. Above this value, rupture properties are governed by the ability of some of the chains to crystallize when stretched. The largest P(%), the highest the maximal crystal volume fraction, and the highest the elongation at break. Below P(%) < 17%, the material cannot crystallize and the rupture properties are governed by the maximal extensibility of the EAC. Thus, the data of non-aged NR2.5 and NR2 aged 7 days in Fig. 12 are explained by their specific EAC length distribution which enables the material to reach the stretch ratio at the crystallization onset. The minimum value of 17% needed for the material to crystallize under strain may be related to the EAC fraction needed to create a phase which can reach λ_c = 4. Note that these conclusions and in particular the calculation of P(%) are not significantly impacted by the uncertainties on the value of λ_c (for sure below 0.2) , or on the value of $\nu_{critical}$ (we have checked that a variation of 30% of this parameter, even though it changes all the calculated values of P(%), does not change the explanation given for the peculiar behavior of non-aged NR2.5 and NR2 aged 7 days).

Literature, and thermoporosimetry experiments, whose methodology and results have been presented in a previous article [13], suggest the existence of spatial heterogeneities in our materials [44]. More crosslinks are expected around the Zno/ZnS clusters resulting from the vulcanization recipe and the material processing. It seems reasonable to consider that the evolution of the crosslink density, which enlarges the distribution width of the EAC length towards shorter chains, does not erase the existence of spatial heterogeneities. Thus, one can assume that the crystallizing phase remaining in the aged material are made of a part of the continuous phase surrounding the ZnO/ZnS clusters and the most crosslinked chains.

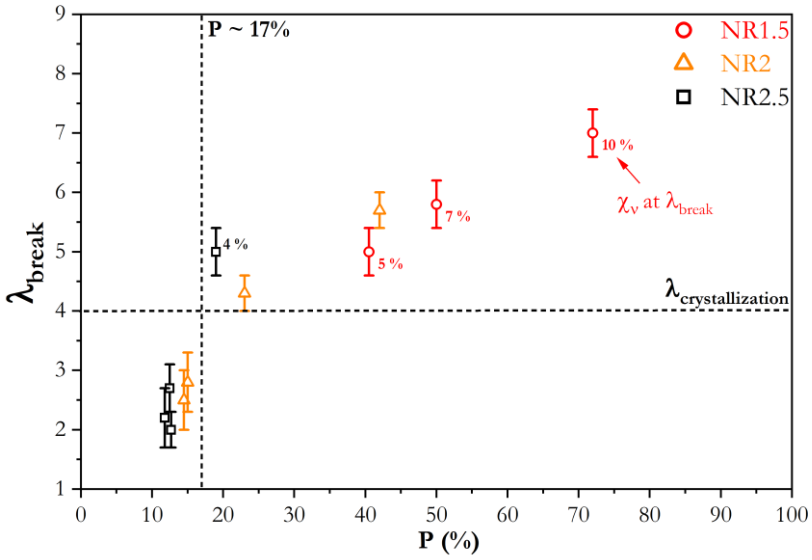

Fig. 13 : Stretch ratio at break as a function of P(%) for NR1.5, NR2 and NR2.5. P(%) represents the proportion of material for which D_{res} is below $D_{res\ critical}$. The number in % represents the crystal volume fraction χ_v measured at λ_{break}

5. CONCLUSIONS

Aged or unaged conventionally crosslinked natural rubbers are far from being model materials to study the relationship between stretch ratio at break and the network structure in elastomer. Nevertheless, the careful examination of their mechanical properties, of their ability to crystallize thermally or under strain, completed by MQ-NMR data enables to understand the evolution of their stretch at break with their ageing. Ageing has obviously consequences on the average EAC density, and on the EAC length distribution. Conversely to the former, this latter is actually not a critical parameter of the evolution of stretch at break in elastomers which do not crystallize (as far as the quantity of free chains and dangling chains stays negligible, which is the case in this study). However, EAC length distribution becomes an important parameter in crystallizable materials like NR, since it will control the quantity of chains which can be stretched enough to crystallize. When this quantity is large enough, the material can be stretched up to λ_c, i.e. up to an elongation ratio at which the crystallization process will enable to increase both the material stretch ratio at break and the stress at break. When the quantity of long chains is too low, whether this is due to the initial crosslinking process or to the material ageing, the elastomer will break at a stretch ratio which is seemingly mainly governed by the average EAC density. A power

law then links both quantities. The found exponent is consistent with other published works (and different from the -0.5 predicted by the Kuhn approach. However, the authors have no really satisfactory explanation to propose for this exponent value.

6. ACKNOWLEDGMENTS

The authors are indebted to Pr. Isabelle Morfin, our local contact at ESRF, for assistance in the experiments on the D2AM line. Besides, we thank Rance Kwamen from Bruker in Germany who performed most of the NMR DQ experiments, Dr. Guilhem Baeza and Prof. Kay Saälwachter for his advices for MQ NMR data treatments.

8. REFERENCES

[1] W. Kuhn, "Dependence of the average transversal on the longitudinal dimensions of statistical coils formed by chain molecules," *J. Polym. Sci. Part a-Polymer Chem.*, vol. 1, no. 5, pp. 380–388, 1946.

[2] Y. Akagi, T. Katashima, H. Sakurai, U. Chung, and T. Sakai, "Ultimate elongation of polymer gels with controlled network structure," *RSC Adv.*, vol. 3, no. 32, p. 13251, 2013.

[3] T. L. Smith, "Strenght and Extensibility of Elastomers," in *Rheology Theory and Applications*, vol. 5, 1969, pp. 127–219.

[4] P. Y. Le Gac, M. Broudin, G. Roux, J. Verdu, P. Davies, and B. Fayolle, "Role of strain induced crystallization and oxidative crosslinking in fracture properties of rubbers," *Polym. (United Kingdom)*, vol. 55, no. 10, pp. 2535–2542, 2014.

[5] A. De Almeida, L. Chazeau, G. Vigier, G. Marque, and Y. Goutille, "Ultimate and toughness properties of γ-irradiated EPDM," *Eur. Polym. J.*, vol. 97, no. June, pp. 178–187, 2017.

[6] J. E. Mark and M.-Y. Tang, "Dependence of the elastomeric properties of bimodal networks on the lengths and amounts of the short chains," *J. Polym. Sci. Polym. Phys. Ed.*, vol. 22, pp. 1849–1855, 1984.

[7] A. Ahagon, "Extensibility of Black Filled Elastomers," *Rubber Chemistry and Technology*, vol. 59, no. 2. pp. 187–203, 1986.

[8] A. G. Thomas, "The development of fracture mechanics for elastomers," *Rubber Chem. Technol.*, vol. 67, no. 3, pp. 50–67, 1994.

[9] G. Lake, “Fatigue and Fracture of Elastomers,” *Rubber Chemistry and Technology*, vol. 68. pp. 435–460, 1995.

[10] G. J. Lake and A. G. Thomas, “The Strength of Highly Elastic Materials,” *Proc. R. Soc. A Math. Phys. Eng. Sci.*, vol. 300, no. 1460, pp. 108–119, 1967.

[11] N. Candau *et al.*, “Influence of strain rate and temperature on the onset of strain induced crystallization in natural rubber,” *Eur. Polym. J.*, vol. 64, pp. 244–252, 2015.

[12] N. Candau, L. Chazeau, J. M. Chenal, C. Gauthier, and E. Munch, “Complex dependence on the elastically active chains density of the strain induced crystallization of vulcanized natural rubbers, from low to high strain rate,” *Polym. (United Kingdom)*, vol. 97, pp. 158–166, 2016.

[13] F. Grasland, L. Chazeau, and J.-M. Chenal, “About thermo-oxidative ageing at moderate temperature of conventionnal vulcanized natural rubber,” *accepted, Polym. Degrad. Stab.*, 2019 . https://doi.org/10.1016/j.polymdegradstab.2018.12.029

[14] P. J. Flory and J. Rehner, “Statistical Mechanics of Cross-Linked Polymer Networks I. Rubberlike Elasticity,” *J. Chem. Phys.*, vol. 11, no. 11, p. 512, 1943.

[15] J. M. Baldwin and D. R. Bauer, “Rubber Oxidation and Tire Aging - A Review,” *Rubber Chem. Technol.*, vol. 81, no. 2, pp. 338–358, 2008.

[16] X. Colin, L. Audouin, J. Verdu, and M. Le Huy, “Kinetic modelling of the thermal oxidation of polyisoprene elastomers. Part 2: Effect of sulfur vulcanization on mass changes and thickness distribution of oxidation products during thermal oxidation,” *Polym. Degrad. Stab.*, vol. 92, no. 5, pp. 898–905, 2007.

[17] S. Trabelsi, “Etude statique et dynamique de la cristallisation des élastomères sous tension,” Orsay, 2002.

[18] J.-M. Chenal and L. Chazeau, “New Insights into the Cold Crystallization of Filled Natural Rubber,” *J. Polym. Sci. Part B Polym. Phys.*, vol. 45, no. April, pp. 1390–1398, 2007.

[19] B. C. Edwards, “The nature of multiple melting transitions in cis-polyisoprene,” *J. Polym. Sci. Polym. Phys. Ed.*, vol. 13, no. 7, pp. 1387–1405, 1975.

[20] M. Akiba, “Vulcanization and crosslinking in elastomers,” *Prog. Polym. Sci.*, vol. 22, no. 3, pp. 475–521, 1997.

[21] L. R. G. Treloar, *The physics of rubber elasticity*, Oxford Uni. USA, 1975.

[22] F. Grasland, L. Chazeau, and J.-M. Chenal, “Which method to quantitatively measure strain-induced crystallization in Natural Rubber?,” submitted to *J. Synchrotron Radiat.*, 2018.

[23] K. Saalwächter, “Modern Magnetic Resonance,” *Springer Int. Publ. AG*, 2017.

[24] K. Saalwächter, “Proton multiple-quantum NMR for the study of chain dynamics and structural constraints in polymeric soft materials,” *Prog. Nucl. Magn. Reson. Spectrosc.*, vol. 51, no. 1, pp. 1–35, 2007.

[25] F. Vaca Chávez and K. Saalwächter, “Time-domain NMR observation of entangled polymer dynamics: Analytical theory of signal functions,” *Macromolecules*, vol. 44(6), pp. 1560–1569, 2011.

[26] K. Saalwächter, B. Herrero, and M. A. Lopez-Manchado, “Chain order and cross-link density of elastomers as investigated by proton multiple-quantum NMR,” *Macromolecules*, vol. 38, no. 23, pp. 9650–9660, 2005.

[27] C. Lorthioir, S. Randriamahefa, and B. Deloche, “Some aspects of the orientational order distribution of flexible chains in a diblock mesophase,” *J. Chem. Phys.*, vol. 139, no. 22, 2013.

[28] W. Chassé, J. L. Valentn, G. D. Genesky, C. Cohen, and K. Saalwächter, “Precise dipolar coupling constant distribution analysis in proton multiple-quantum NMR of elastomers,” *J. Chem. Phys.*, vol. 134, no. 4, pp. 1–11, 2011.

[29] J. Che *et al.*, “Chain dynamics and strain-induced crystallization of pre- and postvulcanized natural rubber latex using proton multiple quantum NMR and uniaxial deformation by in situ synchrotron X-ray diffraction,” *Macromolecules*, vol. 45, no. 16, pp. 6491–6503, 2012.

[30] A. Vieyres *et al.*, “Sulfur-cured natural rubber elastomer networks: Correlating cross-link density, chain orientation, and mechanical response by combined techniques,” *Macromolecules*, vol. 46, no. 3, pp. 889–899, 2013.

[31] H. Kim and L. Mandelkern, “Multiple Melting Transitions in Natural Rubber,” *J. Polym. Sci. Part A-2 Polym. Phys.*, vol. 10, no. 6, p. 1125, 1972.

[32] E. N. Dalal, K. D. Taylor, and P. J. Phillips, “The equilibrium melting temperature of cis-polyisoprene,” *Polymer (Guildf).*, vol. 24, no. 12, pp. 1623–1630, 1983.

[33] N. Candau *et al.*, “Strain-induced crystallization of natural rubber and cross-link densities heterogeneities,” *Macromolecules*, vol. 47, no. 16, pp. 5815–5824, 2014.

[34] J. M. Chenal, L. Chazeau, L. Guy, Y. Bomal, and C. Gauthier, “Molecular weight between physical

entanglements in natural rubber: A critical parameter during strain-induced crystallization," *Polymer (Guildf).*, vol. 48, no. 4, pp. 1042–1046, 2007.

[35] M. Tosaka, "Strain-Induced Crystallization of Crosslinked Natural Rubber As Revealed by X-ray Diffraction Using Synchrotron Radiation," *Polym. J.*, vol. 39, no. 12, pp. 1207–1220, 2007.

[36] J. M. Chenal, C. Gauthier, L. Chazeau, L. Guy, and Y. Bomal, "Parameters governing strain induced crystallization in filled natural rubber," *Polymer (Guildf).*, vol. 48, no. 23, pp. 6893–6901, 2007.

[37] S. Beurrot-Borgarino, "Cristallisation sous contrainte du caoutchouc naturel en fatigue et sous sollicitation multiaxiale," École Centrale de Nantes, 2012.

[38] S. Trabelsi, P. A. Albouy, and J. Rault, "Effective Local Deformation in Stretched Filled Rubber," *Macromolecules*, vol. 36, no. 24, pp. 9093–9099, 2003.

[39] J. L. Valentín *et al.*, "Inhomogeneities and chain dynamics in diene rubbers vulcanized with different cure systems," *Macromolecules*, vol. 43, no. 9, pp. 4210–4222, 2010.

[40] J. L. Valentín, J. Carretero-González, I. Mora-Barrantes, W. Chassé, and K. Saalwächter, "Uncertainties in the determination of cross-link density by equilibrium swelling experiments in natural rubber," *Macromolecules*, vol. 41, no. 13, pp. 4717–4729, 2008.

[41] M. Abdel-Goad, W. Pyckhout-Hintzen, S. Kahle, J. Allgaier, D. Richter, and L. J. Fetters, "Rheological properties of 1,4-polyisoprene over a large molecular weight range," *Macromolecules*, vol. 37, no. 21, pp. 8135–8144, 2004.

[42] Note from the authors : For instance, we found that data of Mark for different polydimethyl siloxanes elastomers with different short chains concentration gives an exponent of -0,6 [6], Akagi found for hydrogel an exponent of -0,65 [2], and Ahagon for SBR and BR an exponent of -0,75 [7]

[43] These spatial heterogeneities cannot be evidence by NMR MQ as it is an averaging technique, and since, for practical reason, we used a unique distribution function for Dres.